PAPER

Automated parallel microassembly for MEMS application

J. Micromech. Microeng. **22** (2012) 035017 (9pp) doi:10.1088/0960-1317/22/3/035017

Automated parallel microassembly for MEMS application

Henry K Chu, James K Mills and William L Cleghorn

Department of Mechanical and Industrial Engineering, University of Toronto, 5 King's College Road, Toronto, Ontario, Canada, M5S 3G8

E-mail: chu@mie.utoronto.ca, mills@mie.utoronto.ca and cleghrn@mie.utoronto.ca

Received 28 October 2011, in final form 5 January 2012
Published 22 February 2012
Online at stacks.iop.org/JMM/22/035017

Abstract
This paper presents the automation of a parallel microassembly process for the construction of out-of-plane microstructures. Images from two vision systems were utilized to automate the grasping and the insertion of three microparts simultaneously. A modified microgripper design and guiding beams were introduced to minimize the possible shift of the micropart and their effectiveness was confirmed experimentally. Parallel microassembly experiments were conducted with success rates of 93% and 61% for the automatic grasping and insertion, respectively. Orientation shifting, experienced by the microparts during the fracture of the supporting tethers, is the suspected cause of failure.

(Some figures may appear in colour only in the online journal)

1. Introduction

Microassembly is the process of assembling microparts into a complicated MEMS device. In general, many microassembly processes are performed under the microscope with a micromanipulation system. To streamline the process, microscope images can be used to provide closed-loop control of the micromanipulation system for automation [1–3]. For instance, Tamadazte *et al* [4] developed a system for automated microassembly of 3D microstructures. CAD models of microparts were first superimposed onto the image and the microparts were manipulated to match with the poses of the models. Das *et al* [5] proposed a hybrid feedforward-feedback control scheme for microassembly. Offline calibration data and visual images were incorporated to assemble microspectrometers with an 80% success rate. Wang *et al* [6] implemented an out-of-plane assembly of polysilicon microparts through a 6-DOF robot manipulator. The assembly practice, from micropart localization to final insertion, was automated through a top-view microscope with a success rate of over 70%. The success of automated microassembly is essential toward the commercialization of assembly-based MEMS devices. Nevertheless, the majority of the research, including the above-mentioned studies, focus on serial processes, which limit the assembly of MEMS devices to one unit at a time. Aiming to improve assembly productivity, this work presents the development of a vision-based, automated parallel microassembly process to assemble multiple MEMS devices simultaneously. Images from two CCD cameras at two different viewpoints were utilized to guide the automatic pick-and-place assembly. This method eliminates the need of CAD model or calibration data in order to perform the assembly process.

In our earlier work [7], a parallel microassembly process was carried out with a manual approach. In the present paper, the parallel grasping and the parallel insertion processes are fully automated. New vision-based algorithms were developed to eliminate the human intervention in these processes. Since the microparts could experience orientation shifts after being grasped by the microgripper as reported in [7], several modifications have been made to the micro-component designs and their effectiveness was examined. In addition, new hardware was added to enhance the system functionality for precise alignment and assembly. A trimetric-view vision system and a visual servoing technique, outlined in [8, 9], were integrated to facilitate the automatic parallel insertion process and the performance of the complete parallel microassembly process was examined experimentally.

2. Background

The process flow of the parallel microassembly is shown in figure 1, and comprises 12 steps to grasp three microparts,

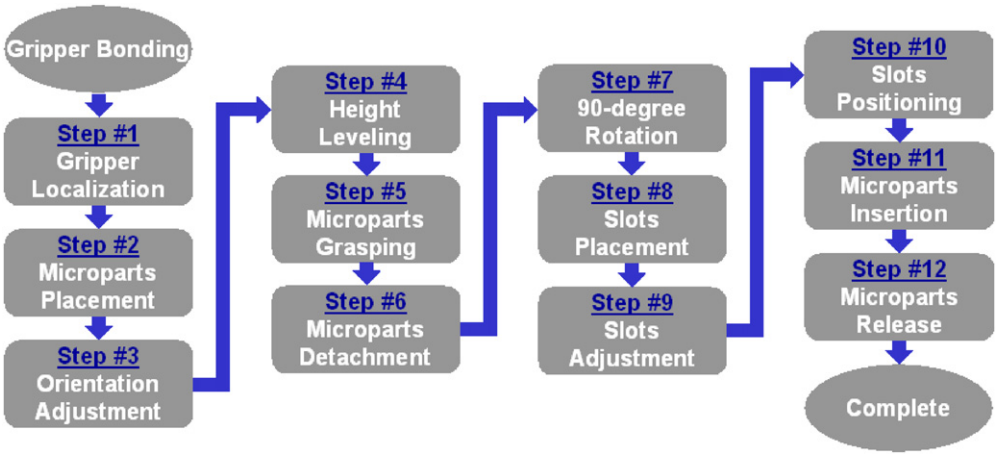

Figure 1. Flow diagram of the parallel microassembly process.

rotate them by 90°, and insert them into the specified slots. A parallel microgripper with three individual grippers was bonded onto an in-house micromanipulation system [7, 8, 10] to conduct the microassembly process. The MEMS chip, containing the microparts and the slots, was placed on the motorized platform for fine positioning. Two vision systems were used to provide images from the top and from a trimetric view, respectively.

In this work, the parallel grasping (steps 3–6) and the parallel insertion (steps 9–12), were automated via a LabVIEW program. In order to automate these steps, new visual-based algorithms and compensation schemes were developed and details are presented in sections 4 and 5. Steps 1, 2 and 8 were performed with the assistance from a human operator to coarsely manipulate the desired micropart and slot sets to the microscope views for the current microassembly operation.

3. Modifications to the micromanipulation system

To enhance the capability of the micromanipulation system in [7] and [8], three key modifications have been made in order to improve the precision for continuous parallel microassembly and to streamline the process.

3.1. Motorized platform

A two-axis goniometer, GN18/M-Z8 from Thorlabs, was added to the system as shown in figure 2. This goniometer provides two extra degrees of rotational motion to the motorized platform for high-precision MEMS chip alignment. When a new MEMS chip is first loaded onto the platform, the chip is pressed gently against the adhesives on the platform to avoid any physical damage. Hence, the MEMS chip may not be level with the platform and the vision system, as shown in figure 3. To precisely align the current MEMS chip under the experiment, the two axes of the goniometer are continuously adjusted until the images from the four corners of the chip are sharp and clear. This indicated that the chip surface is aligned properly with the image plane of the vision system.

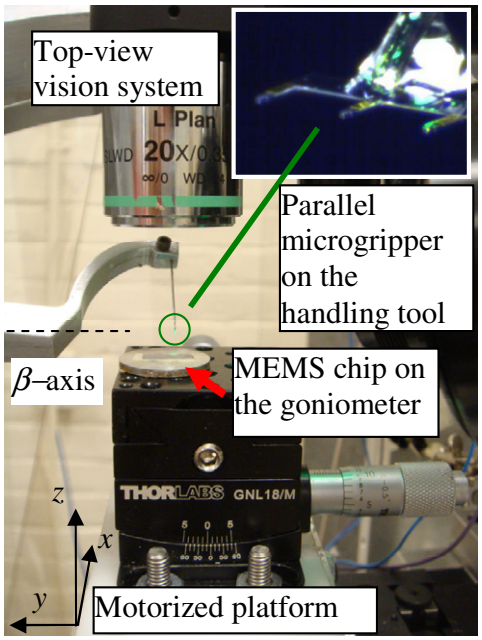

Figure 2. The goniometer on the motorized platform.

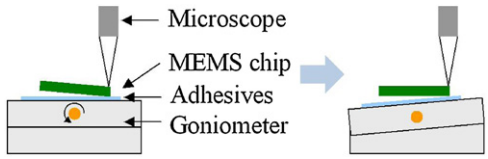

Figure 3. The MEMS chip is (*a*) tilted (exaggerated); (*b*) realigned through the goniometer.

3.2. Micro-components

A modified parallel microgripper was adopted for the microassembly experiments as shown in figure 4. Aiming to minimize the possible orientation shift experienced by the microparts after grasping [7], one modification in the gripper design is to introduce a geometric-matching cavity. The gripper tips and the push beam were redesigned to match with the shape of the hexagonal mating feature on the micropart. Once this hexagon feature is fully grasped by the microgripper,

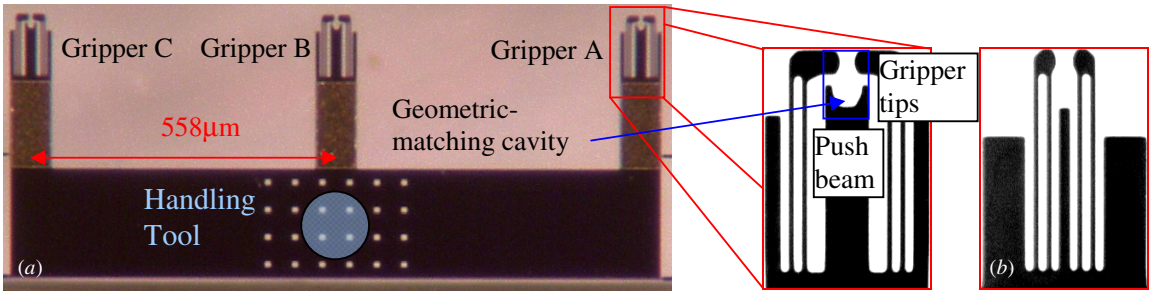

Figure 4. (*a*) Design of the modified parallel microgripper; (*b*) original design in [7].

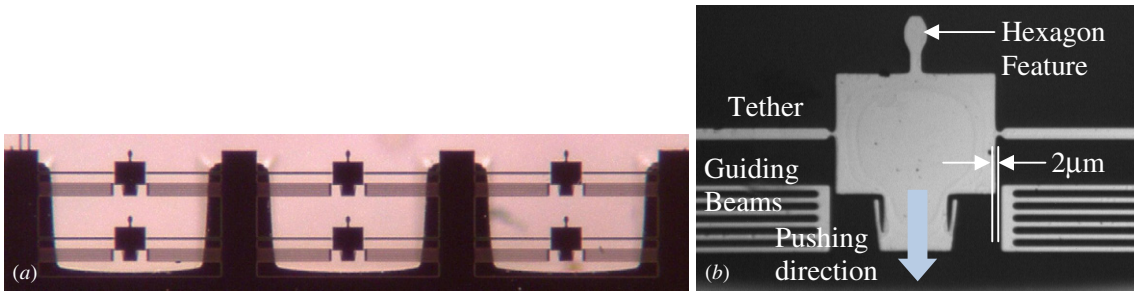

Figure 5. (*a*) Microparts on the MEMS chip; (*b*) details of the micropart.

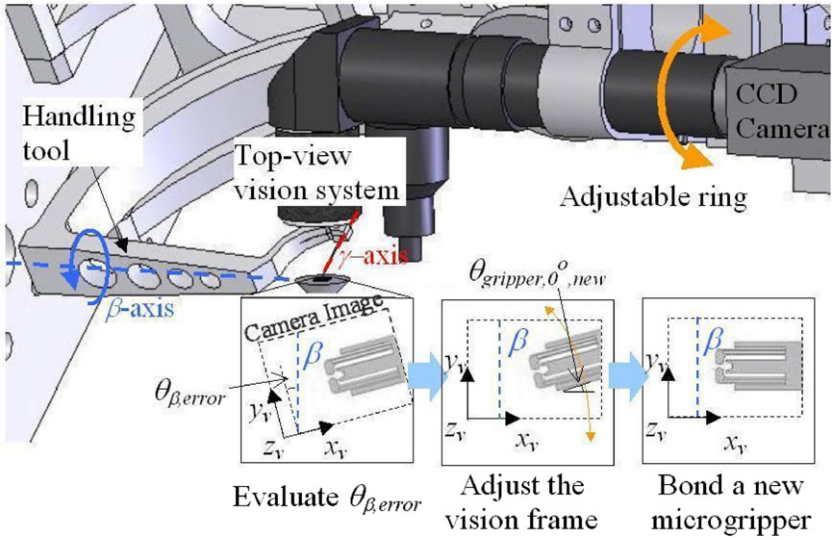

Figure 6. The calibration procedure of the CCD camera.

the geometric-matching cavity will constrain the micropart from shifting during the tether breaking process.

The microparts being grasped by the parallel microgripper are shown in figure 5. Initially, each micropart is suspended on the chip by two 170 μm $\times$ 6 μm tethers. To minimize the shift of the micropart during the tether breaking process, two deflectable guiding beams were also introduced in this work. The presence of these guiding beams constrains the possible shift of the microparts along the pushing direction. Each guiding beam consists of six 170 μm $\times$ 3 μm cantilever beams that are connected together, as shown in figure 5. The effectiveness of the modified microgripper and the guiding beam was examined and the results, in comparing with the original design, are presented in section 6.1.

3.3. CCD camera of the top-view vision system

When performing the out-of-plane rotation, the parallel microgripper on the handling tool of the micromanipulation system is rotated 90° along the rotational axis, β, as shown in figure 6. Initially, the top-view vision system, with a frame (x_v, y_v, z_v) for the captured image, is configured so that the vision y_v-axis is roughly aligned with the β-axis. The orientation of the parallel microgripper is also configured to be aligned orthogonally with the vision system. Nevertheless,

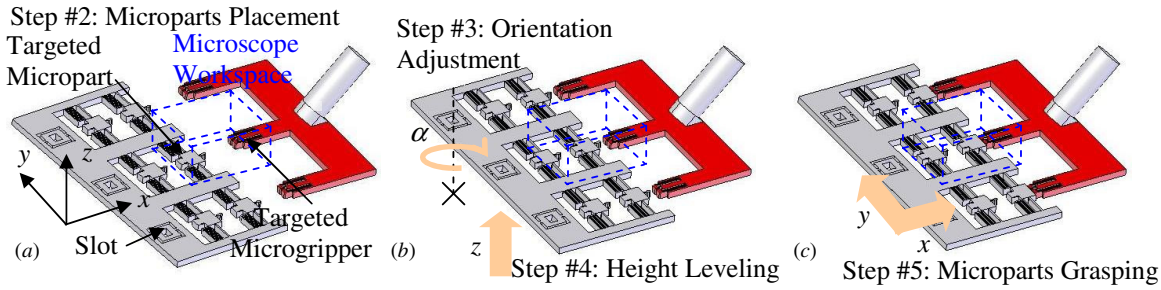

Figure 7. (*a*) The micropart is coarsely positioned within the microscope; (*b*) the micropart is adjusted and leveled with the microgripper; (*c*) the microgripper grasps and detaches the micropart.

misalignment between the y_v-axis and the β-axis, denoted as $\theta_{\beta,\text{error}}$, may exist if the camera is not mounted properly on the microscope tube. Such misalignment may result in significant height deviation between adjacent grasped microparts after 90° rotation. In [7], this misalignment angle was first evaluated and the orientation of the microgripper was physically corrected through the γ-axis of the handling tool in every assembly trial. To streamline the process, this work proposed a calibration scheme for the CCD camera to eliminate the need of γ-axis correction. Since the adjustable ring permits the camera to rotate freely along the vision z_v-axis, the camera was first rotated until the orientation of the microgripper, with respect to the vision frame, corresponded to the new calibrated angle, $\theta_{\text{gripper},0^\circ,\text{new}}$. This adjustment essentially aligned the vision frame with the β-axis, as shown in figure 6. The new calibrated angle, $\theta_{\text{gripper},0^\circ,\text{new}}$, was computed using equation (2) and the orientation of the microgripper at 0° ($\theta_{\text{gripper},0^\circ}$) and at 180° ($\theta_{\text{gripper},180^\circ}$) in the equation were evaluated through the technique discussed in [7]. Following this, a new microgripper was then bonded and this microgripper will now align with both the vision frame and the β-axis:

$$\theta_{\beta,\text{error}} = \frac{\theta_{\text{gripper},0^\circ} - (180 - \theta_{\text{gripper},180^\circ})}{2} \quad (1)$$

$$\theta_{\text{gripper},0^\circ,\text{new}} = \theta_{\text{gripper},0^\circ} - \theta_{\beta,\text{error}} \quad (2)$$

where $\theta_{\beta,\text{error}}$ is the misalignment angle between the vision y_v-axis and the β-axis, $\theta_{\text{gripper},0^\circ}$ is the orientation of the microgripper at 0°, $\theta_{\text{gripper},180^\circ}$ is the orientation of the microgripper after 180° rotation through the β-axis, $\theta_{\text{gripper},0^\circ,\text{new}}$ is the required orientation of the microgripper for calibration.

4. Automatic parallel gasping

Figure 7 illustrates steps 3–6 of the automated grasping process. The middle gripper and the middle micropart in the parallel sets were selected as the targets for vision monitoring, as shown in figure 7(*a*). Once the micropart was coarsely manipulated within the microscope workspace, the orientation discrepancy between the micropart and the microgripper was corrected through the α-axis of the motorized platform. The micropart was then brought to the same height level with the parallel microgripper, as shown in figure 7(*b*). The evaluation and correction techniques involved in these two steps were reported in [7] and the motorized platform was now automated to implement these steps. After that, the micropart manipulated toward the microgripper for grasping and detachment. The techniques reported in [7] were replaced with new vision-based algorithms to assist in the alignment and automation.

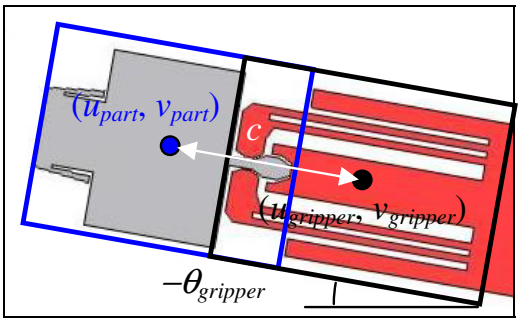

Figure 8. The microgripper grasps the micropart at an angle.

4.1. Automatic grasping

Visual images from the top-view vision system were utilized and the image coordinates of the targeted microgripper and the micropart, $(u_{\text{gripper}},v_{\text{gripper}})$ and $(u_{\text{part}},v_{\text{part}})$, were evaluated using the IMAQ Match Pattern algorithm in LabVIEW [11]. The orientation of the microgripper, θ_{gripper}, was also evaluated and then fed back to the controller of the motorized platform for automatic grasping. A proportional gain constant, K_p, was included in the controller to set the grasping speed. Similar to many visual servoing approaches [12, 13], an interaction matrix, R, was adopted to relate the motions of the micropart in the image with the manipulator motions (platform). This matrix can be evaluated using the intrinsic and extrinsic parameters of the vision system or through experiments. When the micropart was completely grasped by the microgripper, the centroids of the two components did not coincide. A short displacement, c, between the micropart and microgripper resulted, as illustrated in figure 8. This displacement was dependent on the geometry of the micro-components and could be obtained from experiments. For precise grasping, this displacement was decomposed into its x and y components and the manipulator inputs $(\Delta x_{\text{motor}}, \Delta y_{\text{motor}})$ for automatic grasping become

$$\begin{bmatrix}\Delta x_{\text{motor}} \\ \Delta y_{\text{motor}}\end{bmatrix} = K_p R \begin{bmatrix}u_{\text{gripper}} - u_{\text{part}} - c\cos(-\theta_{\text{gripper}}) \\ v_{\text{gripper}} - v_{\text{part}} - c\sin(-\theta_{\text{gripper}})\end{bmatrix} \quad (3)$$

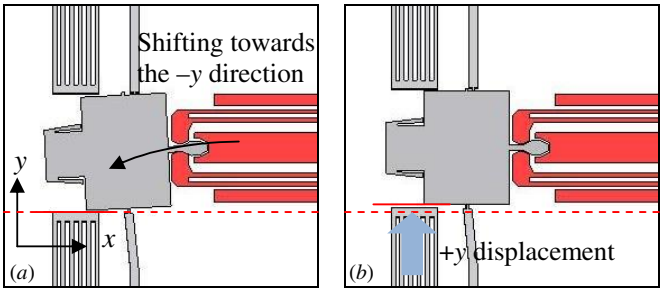

Figure 9. (*a*) The micropart shifts toward the remaining tether in support; (*b*) the micropart is reoriented through the *y*-axis displacement.

where Δx_{motor}, Δy_{motor} are the manipulator inputs in microns, K_p is the gain constant, R is the interaction matrix, (u_{gripper}, v_{gripper}) are the image coordinates of the microgripper, (u_{part}, v_{part}) are the image coordinates of the micropart, c is the displacement in pixels between the microgripper and the micropart when fully grasped, θ_{gripper} is the orientation of the microgripper with respect to the vision frame.

4.2. Automatic detachment

After parallel grasping, the motorized platform was moved in increments of 1 μm for a total of 40 μm to detach the microparts from the two supporting tethers. During this tether breaking process, the two tethers may not sever simultaneously. The micropart would then rotate toward the remaining tether as the platform continued to advance forward to sever the remaining tether, as shown in figure 9(*a*). To minimize the rotational shift imparted onto the micropart, two corrective approaches were examined. The first approach was to add guiding beams to constrain the rotation experienced by the micropart, as shown previously in figure 5. The second approach was to track and reorient the micropart through the *y*-axis of the manipulator. As the micropart is shifting toward one side of the tethers, the motorized platform will impose a linear displacement in the opposing *y*-axis direction to reorient the micropart again, as illustrated in figure 9(*b*). The controller for detachment with this *y*-tracking approach becomes

$$\begin{bmatrix}\Delta x_{\text{motor}}\\ \Delta y_{\text{motor}}\end{bmatrix} = K_p R \begin{bmatrix}0\\ v_{\text{gripper}} - v_{\text{part}} - c\sin(-\theta_{\text{gripper}})\end{bmatrix} + \begin{bmatrix}1\\0\end{bmatrix} \quad (4)$$

where $\begin{bmatrix}1\\0\end{bmatrix}$ is the 1 μm displacement input to the platform.

5. Automatic parallel insertion

The parallel insertion process, from steps 9–12 as shown in figure 10, was automated through the top and the trimetric-view cameras. After the targeted slot was coarsely manipulated to the microscope workspace, the orientation of the slot was corrected through the α-axis of the motorized platform. The slot was then positioned underneath the micropart for insertion. In our earlier work [7], the position alignment process was performed through the top-view images. This process involved locating the micropart tip from the images; however, this process was sensitive to image noises such as background brightness. In this work, the alignment was performed through the trimetric-camera images as discussed in [8]. The visual servoing algorithm presented in [8] was enhanced to compensate position drift of the gripper for precise insertion and the feasibility for parallel insertion of three microparts was examined. Two tracking features, the slot and the micropart reflection on the chip, were tracked and servoed to their desired locations, denoted as ($u_{\text{slot,desired}}$, $v_{\text{slot,desired}}$) and ($u_{\text{reflection,desired}}$, $v_{\text{reflection,desired}}$), as shown in figure 11.

During the entire microassembly process, the positioning stage of the trimetric camera was locked securely. Theoretically, the microgripper image should remain at the same position throughout the subsequent experiments. Nevertheless, the microgripper drifted from its starting position over time. One known reason for the drift is due to the repeatability error of the motor. During each experiment, the microgripper attached to the β-axis must be rotated 90° back and forth. Such motion, coupled with mechanical backlash, would result errors when repositioning the microgripper back to the same position. A repeatability test was conducted and the microgripper position varied by 5 pixels in 10 back-and-forth trials. Another possible reason is due to the thermal effects on the system. Even with this system was set idle, the position of the microgripper shifted by up to 5 pixels in one hour due to the temperature change.

The presence of position drift results in inaccurate evaluation of the desired locations from the learning image. To compensate for the position drift, the current position of the microgripper, ($u_{\text{gripper,current}}$, $v_{\text{gripper,current}}$), was also evaluated in each experiment, as shown in figure 12. The position difference between the microgripper in the current image and in the learning image, ($u_{\text{gripper,learning}}$, $v_{\text{gripper,learning}}$), was computed,

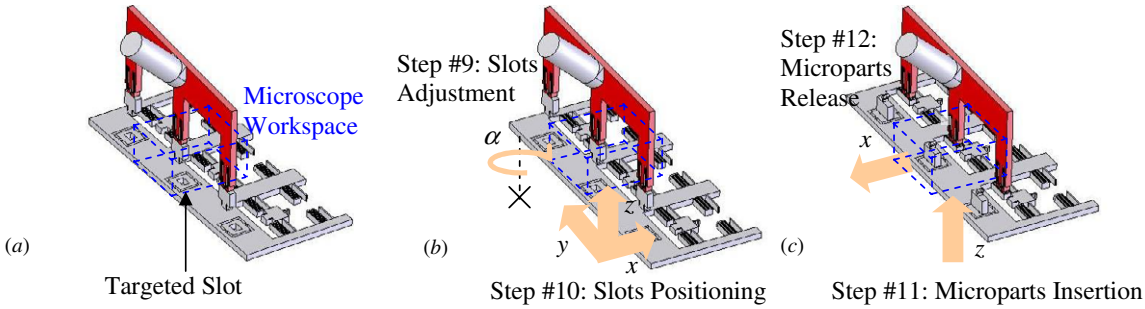

Figure 10. (*a*) The microgripper rotates 90° for out-of-plane insertion; (*b*) the slots are manipulated and aligned with the microparts; (*c*) the microgripper inserts and then releases three microparts.

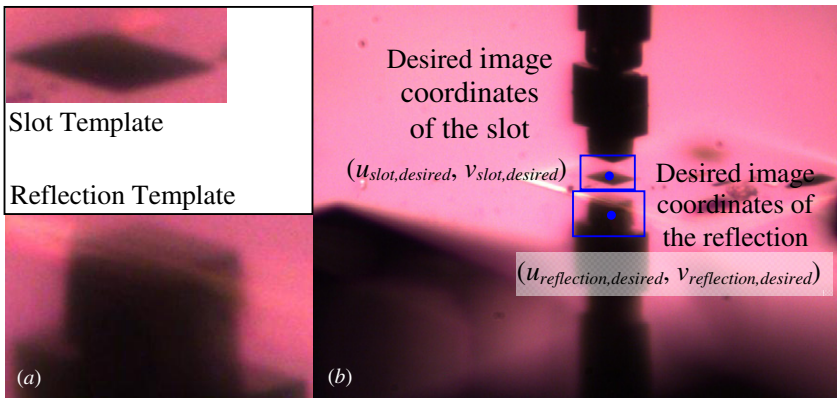

Figure 11. (*a*) Templates used for visual servoing; (*b*) learning image used to evaluate the desired locations of the two features.

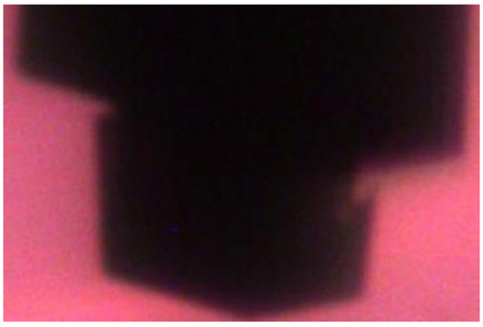

Figure 12. Template of the microgripper.

and the desired locations of the two tracking features, ($u_{\text{slot,new}}$, $v_{\text{slot,new}}$) and ($u_{\text{reflection,new}}$, $v_{\text{reflection,new}}$), were updated as

$$\begin{bmatrix} u_{\text{slot,new}} \\ v_{\text{slot,new}} \\ u_{\text{reflection,new}} \\ v_{\text{reflection,new}} \end{bmatrix} = \begin{bmatrix} u_{\text{slot,desired}} \\ v_{\text{slot,desired}} \\ u_{\text{reflection,desired}} \\ v_{\text{reflection,desired}} \end{bmatrix} + \begin{bmatrix} u_{\text{gripper,current}} - u_{\text{gripper,learning}} \\ v_{\text{gripper,current}} - v_{\text{gripper,learning}} \\ u_{\text{gripper,current}} - u_{\text{gripper,learning}} \\ v_{\text{gripper,current}} - v_{\text{gripper,learning}} \end{bmatrix} \quad (5)$$

where ($u_{\text{slot,new}}$, $v_{\text{slot,new}}$) are the desired image coordinates of the slot after update, ($u_{\text{reflection,new}}$, $v_{\text{reflection,new}}$) are the desired image coordinates of the micropart reflection after update, ($u_{\text{slot,desired}}$, $v_{\text{slot,desired}}$) are the image coordinates of the slot in the learning image, ($u_{\text{reflection,desired}}$, $v_{\text{reflection,desired}}$) are the image coordinates of the micropart reflection in the learning image, ($u_{\text{gripper,current}}$, $v_{\text{gripper,current}}$) are the image coordinates of the microgripper in the current experiment, ($u_{\text{gripper,learning}}$, $v_{\text{gripper,learning}}$) are the image coordinates of the microgripper in the learning image.

6. Experimental results and discussion

6.1. Performance of the modified micro-component designs

The effectiveness of the modified microgripper design and the guiding beams to minimize the rotational shift of the micropart during the tether breaking process were studied with four scenarios, as summarized in table 1. In order to isolate other factors that could influence the micropart grasping performance, the parallel microgripper only grasped a single micropart through the middle gripper in each trial. The two adjacent microparts were removed prior to experiments to prevent any imbalance forces imparted onto the parallel microgripper due to misalignment or unsuccessful grasping from affecting the middle gripper. In the first two scenarios, the two microgripper designs were examined with the *y*-tracking algorithm. In the next two scenarios, the performance of guiding beams to replace the *y*-tracking algorithm was studied. For each scenario, six trials were conducted and the evaluated angular orientations (0–360°) of microgripper and the micropart from the top-camera after detachment were summarized in table 2.

Table 1. Summary of the four scenarios.

	Gripper design	Detachment
Scenario 1	Original	*y*-tracking
Scenario 2	Modified	*y*-tracking
Scenario 3	Original	Guiding beams
Scenario 4	Modified	Guiding beams

When performing the grasping experiments, sudden, exaggerated shifting of the micropart was experienced. The values indicated in bold in table 2 represent the results of these occurrences. One possible reason is due to the quality of the fabricated MEMS chip. Miller *et al* in [14] examined the fracture strength of various micro-fabrication technologies. For the SOIMUMPs fabrication technique selected in this work, individual defects, ranged from 100 to 200 nm in depth, were observed on the top surface of the processed silicon wafers. The depths of these defects are dependent on the etch time of the silicon wafers and these individual defects could result in greater variability on the material's fracture strength. Due to the inconsistency of the fracture strength, microparts fabricated on the area that require higher assembly force to break the two supporting tethers are susceptible to experiencing a higher level of shifting.

To evaluate the performance of the micro-component designs, the outlying data were omitted when calculating the average orientation shift of the micropart for each scenario. The Chauvenet's criterion was used to examine whether or not the measured value was considered as a statistical outlier.

Table 2. The angular orientations of the micro-components after grasping.

		Set 1 (°)	Set 2 (°)	Set 3 (°)	Set 4 (°)	Set 5 (°)	Set 6 (°)	$\lvert X_{avg}\rvert$ (°)
Scenario 1	Gripper	0.38	359.63	359.49	359.67	0.01	359.1	
	Part	2.03	358.35	359.23	358.5	4.08	356.4	
	Delta (X_i)	−1.65	1.28	0.26	1.17	**−4.07**	2.7	1.86
Scenario 2	Gripper	359.84	359.9	359.73	359.7	0.8	359.6	
	Part	358.67	359.98	358.2	358.85	7.07	0.43	
	Delta (X_i)	1.17	−0.08	1.53	0.85	**−6.27**	−0.83	1.79
Scenario 3	Gripper	359.87	359.97	0.01	359.92	359.99	359.94	
	Part	358.65	0.2	0.16	1.13	359.16	1.41	
	Delta (X_i)	1.22	−0.23	−0.15	−1.21	0.83	−1.47	0.85
Scenario 4	Gripper	0.05	359.8	359.6	359.99	359.98	359.9	
	Part	359.8	0.05	359.76	356.29	1.01	359.6	
	Delta (X_i)	0.25	−0.25	−0.16	**3.7**	−1.03	0.3	0.95

Table 3. The angular orientations of the micro-components after grasping.

		Set 1	Set 2	Set 3	Set 4	Set 5	Set 6	|Avg.| (°)
Scenario 1	τ	0.15	0.43	1.19	0.51	1.65	0.63	
	Delta (X_i)	−1.65°	1.28°	0.26°	1.17°	−4.07°	2.7°	1.86
Scenario 2	τ	0.28	0.76	0.11	0.42	1.99	0.43	
	Delta (X_i)	1.17°	−0.08°	1.53°	0.85°	/	−0.83°	0.89
Scenario 3	τ	0.67	1.13	1.27	0.65	0.04	1.12	
	Delta (X_i)	1.22°	−0.23°	−0.15°	−1.21°	0.83°	−1.47°	0.85
Scenario 4	τ	0.50	0.50	0.57	1.99	0.06	0.47	
	Delta (X_i)	0.25°	−0.25°	−0.16°	/	−1.03°	0.3°	0.33

The mean, X_{avg}, and the standard deviation, s_x, from the six measured values, X_i, in each scenario were calculated to evaluate the nondimensional deviation, τ, using equation (6). According to Chauvenet's criterion for measurement with six datum points, if a datum point has a τ value higher than 1.73, such point is considered to be outside the 91.7% probability band about the mean and could be omitted from calculation [15, 16]. Based on this criterion, two datum points, one in scenario 2 and one in scenario 4, were omitted and the average orientation shift was calculated and summarized in table 3.

When comparing the average values obtained in scenarios 1 and 2, the incorporation of the modified microgripper design can reduce the rotational shift of the micropart from 1.86° to 0.89°. The guiding beam design was also proven to be a more effective approach than the *y*-tracking algorithm to minimize the shift of the micropart. Together with the modified microgripper design, the orientation variation can then be minimized to 0.33°. Since this combination yielded the best grasping performance, these two implementations were adopted to conduct the automatic parallel microassembly operations.

$$\tau = \left| \frac{X_i - X_{avg}}{s_x} \right| \quad \text{for } i = 1\text{–}6 \tag{6}$$

where τ is the nondimensional deviation, X_i is the measured value for set *i*, X_{avg} is the mean of the measured values, s_x is the standard deviation.

6.2. Performance of the automatic parallel grasping process

The parallel grasping process was performed as outlined in section 4 and figure 13 shows the snapshots of the experiment. The average time to complete these steps is approximately 60 s. Ten trials were conducted with 30 microparts to be grasped. Experiment results from five different MEMS chips show that 28 microparts were successfully grasped and the overall success rate was approximately 93%. During the experiments, one of the observed failures was due to the guiding beams. The corner of the micropart collided with the guiding beam and hence, failed to be grasped securely by the gripper after detachment.

6.3. Performance of the automatic parallel insertion process

The automatic parallel insertion was then performed and figure 14 shows the images from the trimetric camera. The average time to complete the automatic insertion is 144 s. For the 28 microparts grasped from the ten trials, only 17 were successfully inserted into the slots, which corresponded to a success rate of 61%. Majority of the parallel insertion failures occurred at the two microparts which were not visually monitored. For the targeted micropart, the success rate was 90%.

The primary reason for this failure is due to the orientation variation of the grasped microparts, as examined in section 6.1. Significant orientation deviation between these microparts would then result in unexpected error in the parallel slot alignment and positioning through the tracking micropart. In addition, undesired vertical shift also occurred. As observed from the experiments, the microgripper deflected downward and became out-of-focus when pushing the micropart forward, as illustrated in figures 15(*a*) and (*b*). As one of the two tethers was severed, the induced assembly force on the parallel microgripper was reduced and microgripper returned to the same horizontal level as the chip. However, if the

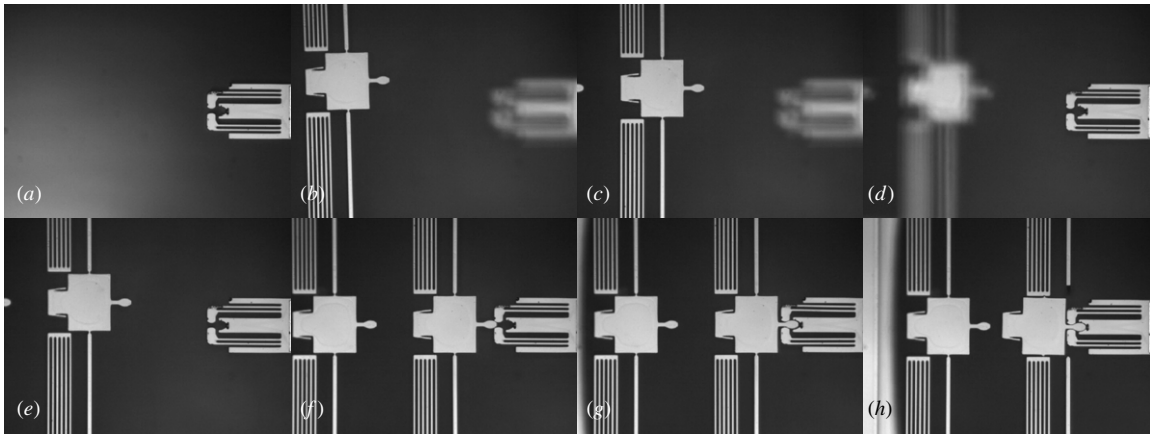

Figure 13. (*a*) Microgripper appears on the image; (*b*) micropart is in focus; (*c*) micropart corrects its orientation through the α-axis; (*d*) microgripper is back in focus; (*e*) micropart levels with the microgripper; (*f*) micropart is manipulated toward the microgripper; (*g*) microgripper grasps the micropart; (*h*) micropart releases from the supporting tethers.

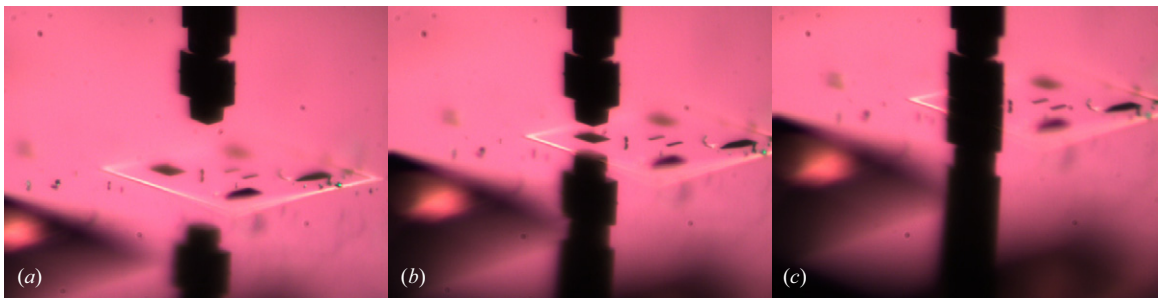

Figure 14. (*a*) The slot is at the initial position for the experiment; (*b*) the slot is servoed to the desired location; (*c*) the micropart is inserted into the slot.

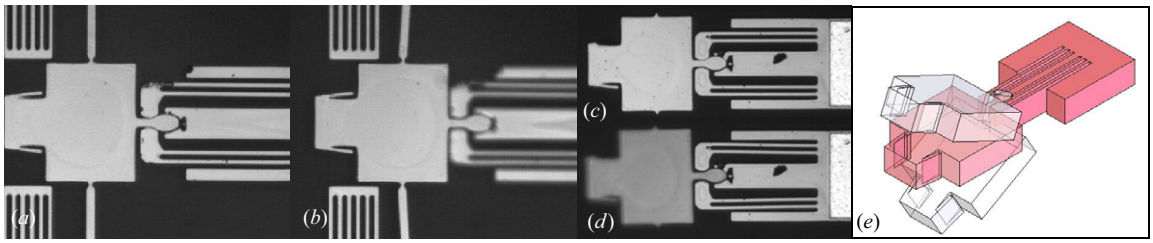

Figure 15. (*a*) The microgripper grasps the micropart; (*b*) the microgripper bends downward when trying to break the tether; (*c*) the microgripper and the micropart are at the same level after detachment; (*d*) the micropart is vertically shifted and is not as sharp as the microgripper; (*e*) schematic shows the possible vertical shift of the grasped micropart.

micropart was detached from the remaining tether before the microgripper vertical position was corrected, the grasped micropart would be tilted upward and was seen to be out-of-focus, as shown in figure 15(*d*).

Since the orientation of the grasped microparts contributes significantly to the success rate of automated the parallel insertion process, it is advised to impose further constraints to the shifting of the microparts. One approach is to use a fixture to correct the orientation of the microparts after grasping. The concept of using MEMS fixtures in assembly was also considered by Tahhan *et al* in [17]. The purpose of the fixture in this work is to realign the orientation of each micropart as they are engaged with the fixture. The fixture was constructed by cutting three notches from the MEMS chip, as shown in figure 16. The edges on the notches were

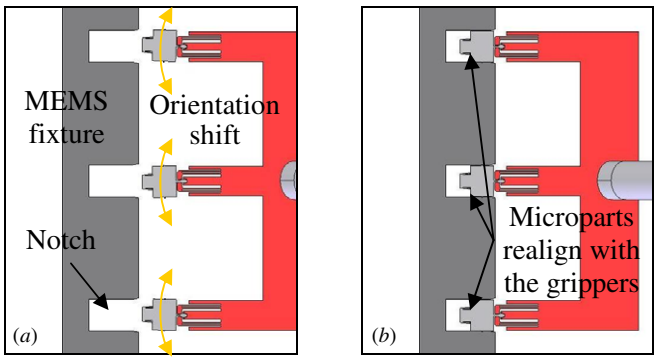

Figure 16. The parallel microgripper with microparts: (*a*) approaches the fixture; (*b*) inserts into the fixture.

tapered to facilitate insertion of the microparts into the fixture. Preliminary result shows that the adhesive force between the micropart and the fixture could prevent the microparts from engaging with the notches. Hence, further parametric studies on the notch design should be conducted to examine the effectiveness for realignment. Another potential approach is to apply a larger grasping force onto the microparts. To support larger forces, the microgripper could be fabricated with different materials to increase the overall stiffness. A multilayer interlocking mechanism between the microgripper and the micropart, proposed in [18], could also be incorporated to minimize the possible vertical misalignment as shown in figure 15(*e*).

7. Conclusion

This work demonstrates an automatic microassembly of three out-of-plane microstructures with a micromanipulation system. In order to ensure precise orientation alignment between the grippers and the microparts, a modified microgripper design and guiding beams were introduced to minimize the possible shift of the micropart throughout the process. Results from experiments show that the orientation deviation can be kept within 0.33° on average.

The automatic parallel grasping process was examined in ten trials. A success rate of 93% was achieved and the process completed in 60 s on average. Automatic parallel insertion was then performed. Results show that the three microparts can be simultaneously inserted into the slots in 144 s with a success rate of 61%. Failure in the parallel insertion occurs mainly at the two outermost microparts which are not monitored. Orientation variation between the grasped microparts is considered as the primary cause for this failure. With the three microparts no longer in the same orientation, the alignment and positioning strategies performed on the selected microgripper may not be applicable to the remaining microgrippers.

References

[1] Nelson B J, Zhou Y and Vikramaditya B 1998 Sensor-based microassembly of hybrid MEMS devices *IEEE Control Syst.* **18** 35–45

[2] Sulzmann A, Breguet J M and Jacot J 1997 Micromotor assembly using high accurate optical vision feedback for microrobot relative 3D displacement in submicron range *Proc. Int. Conf. Solid State Sensors and Actuators* pp 279–82

[3] Heriban D and Gauthier M 2008 Robotic micro-assembly of microparts using a piezogripper *IEEE/RSJ Int. Conf. on Intelligent Robots and Systems* pp 4042–7

[4] Tamadazte B, Marchand E, Dembele S and Le Fort-Piat N 2010 CAD model-based tracking and 3D visual-based control for MEMS microassembly *Int. J. Robot. Res.* **29** 1416–34

[5] Das A N, Popa D O and Stephanou H E 2010 Automated microassembly using precision based hybrid control *Proc. IEEE Int. Conf. on Robotics and Automation* pp 4106–12

[6] Wang L, Mills J K and Cleghorn W L 2008 Automatic microassembly using visual servo control *IEEE Trans. Electron. Packag. Manuf.* **31** 316–25

[7] Chu H K, Mills J K and Cleghorn W L 2010 Parallel microassembly with a robotic manipulation system *J. Micromech. Microeng.* **20** 125027

[8] Chu H K, Mills J K and Cleghorn W L 2011 Image-based visual servoing through micropart reflection for microassembly process *J. Micromech. Microeng.* **21** 065016

[9] Chu H K, Mills J K and Cleghorn W L 2010 Dynamic tracking of moving objects in microassembly through visual servoing *Proc. IEEE Int. Conf. on Mechatronics and Automation* pp 1738–43

[10] Dechev N, Cleghorn W L and Mills J K 2006 Development of a 6 DOF robotic micromanipulator for use in 3D MEMS microassembly *Proc. IEEE Int. Conf. on Robotics and Automation* pp 281–8

[11] National Instruments 2003 IMAQ Vision for LabVIEW User Manual, available at http://www.ni.com/pdf/manuals/371007a.pdf

[12] Hutchinson S, Hager G D and Corke P I 1996 A tutorial on visual servo control *IEEE Trans. Robot. Autom.* **12** 651–70

[13] Ren L, Wang L, Mills J K and Sun D 2008 Vision-based 2D automatic micrograsping using coarse-to-fine grasping strategy *IEEE Trans. Ind. Electron.* **55** 3324–31

[14] Miller D C, Boyce B L, Dugger M T, Buchheit T E and Gall K 2007 Characteristics of a commercially available silicon-on-insulator MEMS material *Sensors Actuators* A **138** 130–44

[15] Coleman H W and Glenn Steele W 2009 *Experimentation, Validation, and Uncertainty Analysis for Engineers* (Hoboken, NJ: Wiley) chapter 2 pp 47–51

[16] Schenck H 1979 *Theories of Engineering Experimentation* (United States: Hemisphere Publishing Corporation) chapter 8 pp 228–34

[17] Tahhan I N, Zhuang Y, Bohringer K F, Pister K S J and Goldberg K 1999 MEMS fixtures for handling and assembly of microparts *Proc. SPIE* V 129–39

[18] Dechev N, Cleghorn W L and Mills J K 2004 Microassembly of 3D microstructures using a compliant, passive microgripper *J. Microelectromech. Syst.* **13** 176–89